Electronic Supplementary Material (ESI) for Journal of Materials Chemistry A.

Enhancement in kinetics of the oxygen reduction on a silver catalyst by introduction of interlaces and defect-rich facets

Xiaohong Xie,[‡ab] Mengxia Wei,[‡a] Lei Du,[bc] Yao Nie,[a] Xueqiang Qi,[a] Yuyan Shao,[b] and Zidong Wei*[a]

[a] School of Chemistry and Chemical Engineering, Chongqing University, Chongqing 400044, China

[b] Pacific Northwest National Laboratory, Richland, Washington 99352, United States

[c] School of Chemistry and Chemical Engineering, Harbin Institute of Technology, Harbin 150001, China

‡ These authors contributed equally to this work

*Corresponding Author: zdwei@cqu.edu.cn

Experimental Section

Chemicals and Materials

$(NH_4)_2MoO_4{\cdot}4H_2O$ (99.99%), $NaBH_4$ (99.99%), $AgNO_3$ (99.99%), KOH (99.99%), H_3PO_4 (85%) and HNO_3 (65%) were obtained from Chongqing (China) Chuan-Dong Chemical Reagent Co. Ltd. Nafion (5.0 wt %) was commercially obtained from Sigma-Aldrich. Pt/Carbon (Pt/C) catalyst (40 wt. %) was purchased from Alfa-Aesar. All reagents were all used as received. Aqueous solutions were prepared using deionized (DI) water with a resistivity of 18.2 MΩ cm.

Synthesis of pristine-POM (*POM*, $(NH_4)_3PMo_{12}O_{40}$)

POM was prepared using a previously reported method.[1] In brief, 0.01 mol $(NH_4)_2MoO_4{\cdot}4H_2O$ and 0.012 mol H_3PO_4 were dissolved together in 200 ml of DI water. After vigorous stirring for 15 min, the solution color changed to light green. Then 8 ml of a concentrated HNO_3 was added, drop-by-drop, into the solution and maintained at 80 °C for 2 h. The resulting yellow colloidal product was filtered and washed with 1.0 % HNO_3 solution for several times and vacuum dried at 80 °C.

Synthesis of discrete reduced-POM nanoclusters (*rPOM*)

rPOM was synthesized *via* a chemically reduction route. Briefly, 5 g of POM powder was dispersed in 50 ml of DI water. Then 0.25 g of $NaBH_4$ was added to the above dispersion at room temperature under stirring: as soon as the reduction of the POM occurred, gas evolution ($NH_4^+ + H^- \rightarrow NH_3\ (g) + H_2\ (g)$) occured, and the solution color changed from yellow to dark-blue. After stirred for 2 h to allow the complete reaction of the POM, the rPOM containing solution was diluted with 50 mL of DI water and maintained in the refrigerator at 5°C for 24 h to precipitate the impurities, and then, the upper parts of the resulting solution was isolated and dried in a freezer dryer to obtain the rPOM.

Synthesis of nanoporous Ag catalyst (*np-Ag*)

In a typical synthesis, 1 g of rPOM powder was dissolved in 200 mL of DI water. $AgNO_3$ precursor (0.1 to 0.8 g) was dissolved in 10 ml of water and added drop-wise to the first solution under stirring so that the dark-blue solution soon became slightly cloudy with the formation of a rPOM and Ag^+ (rPOM-Ag(I)) intermediate composite. The reaction mixture was then stirred for 30 min and heated to 95 °C for another 2 h before it was cooled to ambient temperature. After the completion of the reaction, the resulting product was filtered, washed with 0.1 M KOH solution and water for several times and dried in a vacuum (80 °C). A separated intermediate of rPOM-Ag(I) was also synthesized and separated according to the same method as that used to prepare the np-Ag, except without heat treatment. For catalyst comparison, 40 wt% Ag support on C (Ag/C) was prepared by applying the $NaBH_4$ method.[2]

Instruments:

The X-ray diffraction (XRD) data were collected on a XRD-6000 using Cu KR radiation at a scan speed of 2° min^{-1}. The Fourier Transform IR Spectroscopy (FT-IR) spectra were recorded on a Nicolet 550II FT-IR spectrometer. X-ray photoelectron spectroscopy (XPS) was tested on a Cratos XSAM800 spectrometer equipped with a monochromatic Al X-ray source (Al KR, 1.4866 keV), and the binding energy was calibrated using 285 eV as the C 1s peak binding energy. Transmission electron microscopy (TEM) and high-resolution transmission electron microscopy (HRTEM) were conducted on a FEI tecnai instrument operating at 120 kV. Scanning electron microscopy (SEM) and corresponding energy-dispersive X-ray (SEM-EDX) measurements were performed on a LEO-1530VP instrument.

Electrochemical measurements:

All electrochemical experiments were performed using a Princeton electrochemical workstation in a typical three-electrode cell. A leak-free AgCl/Ag/KCl (3 M) electrode (Warner Instruments) was used as the reference electrode. All potentials were converted to values with reference to the RHE. A Pt wire was used as a counter electrode. A glassy carbon (GC) disk electrode with a diameter of 5 mm and geometric area of 0.19625 cm^2 (Pine Instruments) was polished with 0.05 µm alumina before each experiment and used as a working electrode. The electrolyte was placed in 0.1 M KOH solution. For electrode preparation, the catalyst was dispersed in ½ethonal/½DI water and sonicated for 30 minutes to form a uniform catalyst ink, and a certain amount of this ink was loaded onto the GC electrode. After the solvent was evaporated, the deposited catalyst was covered with one drop of dilute aqueous Nafion solution (~ 5 µl, 0.5 wt. %). The resulting thin film was sufficiently strong to permanently attach the catalyst materials to the GC surface without producing resistance. We compared Ag and Pt/C catalysts at different mass loading (637 µg cm^{-2} for np-Ag/GC (125ug Ag on GC electrode) and 63.7 µg cm^{-2} for Pt/C/GC (5 ug Pt on GC electrode)), and the amount of catalyst deposited for the Ag/C catalyst was well adjusted to provide the same electrode of Ag as the np-Ag catalyst. Although the np-Ag catalyst (refer to Ag) on the electrode is 25 times the mass loading of Pt/C (refer to Pt), np-Ag is still comparable to Pt/C at half of the cost (the price of Ag is ~1/50 of Pt).[3] The prepared electrodes were dried at room temperature for 20 minutes before testing. All measurements were conducted 5 times to avoid any incidental error. The kinetic analysis was conducted according to Koutecky-Levich (K-L) plots:

$$\frac{1}{j}=\frac{1}{j_k}+\frac{1}{B\omega^{0.5}}$$

where j_k is the kinetic current and B is Levich slope which is given by:

$$B=0.2nFCD^{2/3}\nu^{-1/6}$$

here n is the number of electrons transferred in the reduction of one O_2 molecule, F is the Faraday's constant (96485 C mol^{-1}), C is the saturated concentration of oxygen (1.2×10^{-3} mol L^{-1}), D is the diffusion coefficient of oxygen in 0.1 M KOH solution (1.9×10^{-5} cm^2 s^{-1}), and ν is the kinematic viscosity of the solution (0.01 cm^2 s^{-1}, 25 °C). The constant 0.2 is adopted when the rotation speed is expressed in rpm.[4]

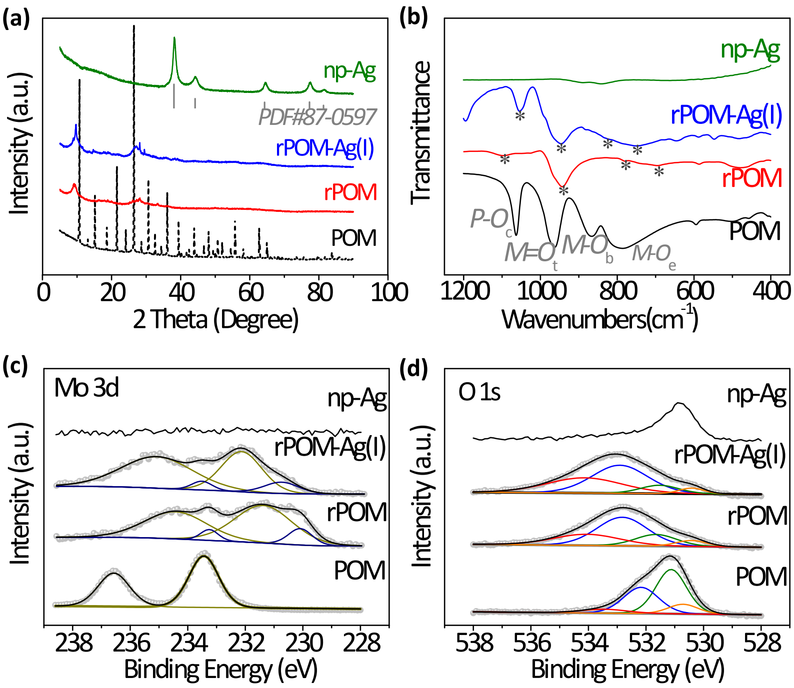

Figure S1. (a) XRD patterns, (b) FTIR spectra, (c) high-resolution Mo 3d XPS spectra and (d) O 1s XPS spectra of as-synthesized materials.

It is noteworthy that POMs are combinations between oxygen and early transition metals (e.g., Mo, W, V, Nb, and Ta). Their molecular frameworks can be regarded as nanoscale metal oxide from both structural and electronic points of view.[5] POMs can accept and release a large number of electrons without changing or decomposing their structural arrangements. The $NaBH_4$ route is able to cause the chemical reduction of POM as well as transform POM into a scale of nanoscale clusters. The purity and structure of as-synthesized materials were determined by XRD measurements. In Figure S1a, all characteristic peaks can be observed in POM, whereas no indexed diffractions corresponding to crystalline phase and structure, can be observed in the reduced form, indicating that the rPOM may contain very small nanoclusters that are not well crystallized; instead, they may be in an amorphous state. When mixed with $AgNO_3$, however, the diffraction pattern of the resulting composite, rPOM-Ag(I), displayed no significant change when compared with rPOM. This result reveals that rPOM-Ag(I) composites are a structure consisting of rPOM peripherally coordinated by Ag^+ ions.

Infrared (IR) spectrometry was employed to elucidate the interaction between Ag^+ and rPOM. A pure POM nanostructure has the following four types of oxygen species: central oxygen (O_c), terminal oxygen (O_t), bridged O of MoO_6 octahedra sharing a corner (O_b), and sharing an edge (O_e). Intense bands at 1068, 962, 869 and 785 cm^{-1} in the Fourier transform IR (FTIR) spectrum of POM (Figure S1b) are assigned to the vibrations of P-O_c, Mo=O_t, Mo-O_b, and Mo-O_e, respectively.[6] In the FTIR spectrum of the converted rPOM, a hypsochromic shift of the P-O_c and bathochromic shifts of the three types of Mo-O are observed, which are compared with pristine POM. Moreover, the spectrum of rPOM shows a dramatic decrease in the band intensities, which is ascribed to the reduction of POM that causes an increase in the electron density of Mo, causing the structural modification in the rPOM. However, the FTIR absorption changes we observed in the rPOM-Ag(I) composites are much smaller than those in rPOM when compared with those in POM. Those observation reflects the coordination, resulting in electrostatic and electronic interaction between rPOM structure and Ag^+ ions. Incorporation of rPOM and Ag^+ will decrease the electron density of rPOM, weakening the structural changes in the rPOM.

The chemical compositions and valence-states of materials were evaluated by XPS measurements. The XPS Mo 3d spectrum of POM (Figure S1c) shows only a Mo doublet that is assigned to Mo(VI) (at its high oxidation state), whereas a significant widening and shift in Mo 3d binding energy was observed in converted rPOM. A detailed inspection of the Mo 3d spectrum of rPOM reveals that it is deconvoluted into two parts that are attributed to Mo at different valence-states, and the peak Mo undergoes a negative shift compared with the POM. This negative shift could, therefore, increase the electron density in Mo and then enhance the electronegativity of the rPOM, making the rPOM have a higher affinity to the Ag^+ ions. Although the Mo 3d spectra of the rPOM-Ag(I) intermediate is similar to that of rPOM, the coupling of rPOM with Ag^+ results in a positive-shift of the Mo 3d binding energy, which verified the decrease in the rPOM electron density for the hybrid composites due to the ligand-interactions. The O 1s patterns are given in Figure S1d to further demonstrate the chemical-states changes in materials. The XPS analysis is consistent with the IR spectral results.

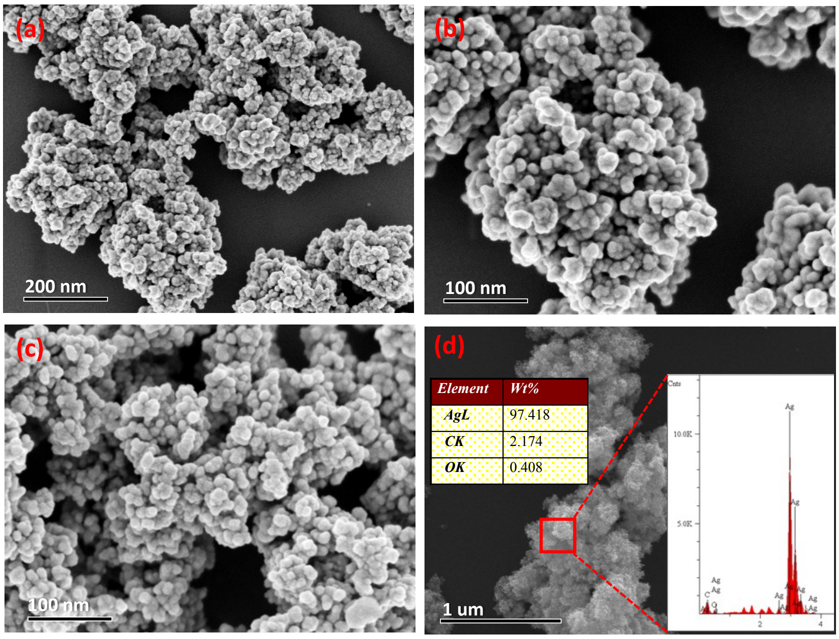

Element	*Wt%*
AgL	97.418
CK	2.174
OK	0.408

Figure S2. (a-c) SEM images of as-formed np-Ag material and the corresponding energy dispersive X-ray spectroscopic (EDX) data from the SEM measurement (d); that for np-Ag is shown in insert (d), and the weight percentages of the elements are shown in the insert.

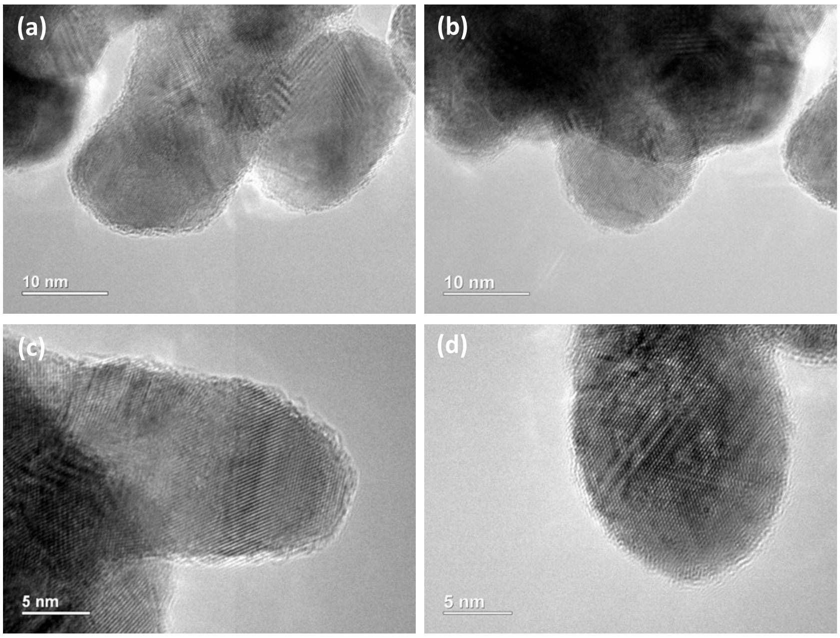

Figure S3. Additional HR-TEM images of np-Ag: different facets/surfaces can be observed in a single Ag nanocrystal.

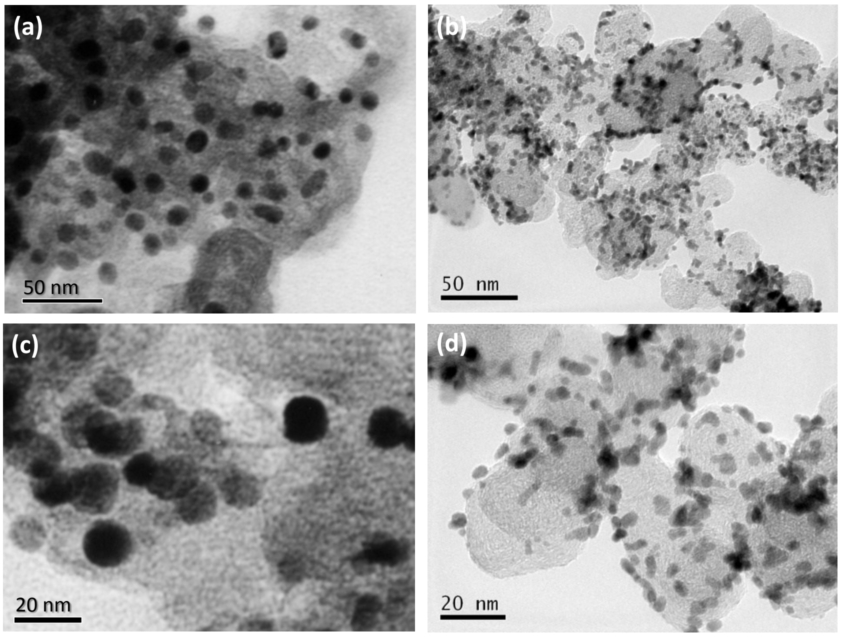

Figure S4. TEM images of (a), (c) Ag/C and (b), (d) commercial Pt/C catalysts. Loading: 40 wt %.

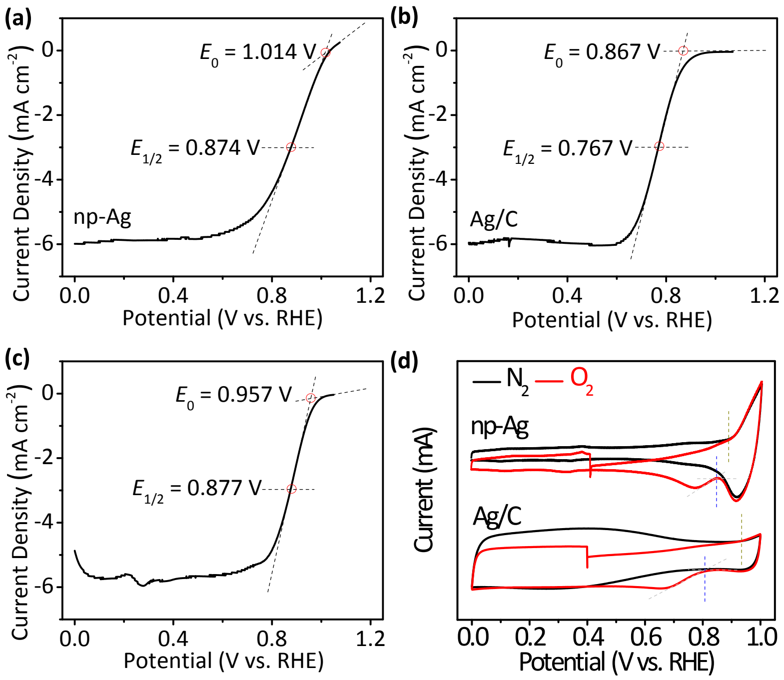

Figure S5. ORR response at (a) np-Ag, (b) Ag/C and (c) Pt/C catalysts in O_2-saturated 0.1 M KOH solution; scan rate: 10 mV s^{-1}; rotation rate: 1600 rpm. (d) CV curves for np-Ag and Ag/C recorded in N_2-saturated and O_2-saturated 0.1 M KOH solution.

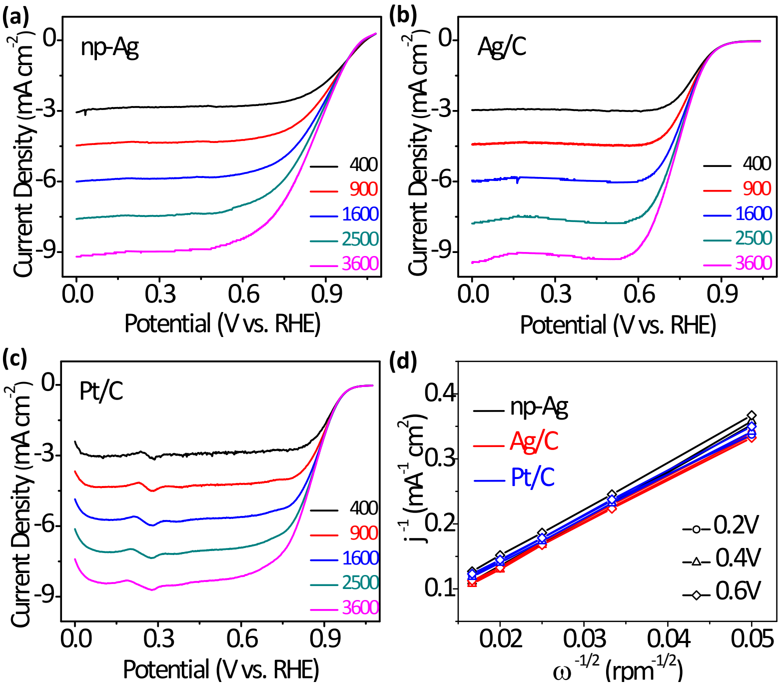

Figure S6. ORR polarization curves at different rotation rate with Koutecky-Levich plots.

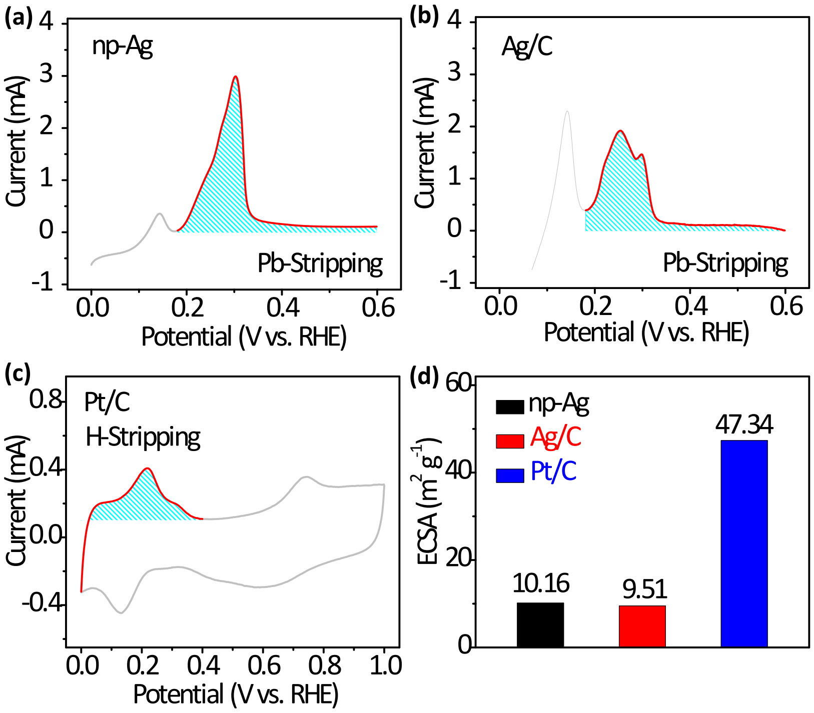

Figure S7. (a) and (b) Pb-stripping voltammograms used to measure the ECSA of np-Ag and Ag/C catalysts at 10 mV s^{-1} in 0.1 M KOH solution with 125 uM $Pb(NO_3)_2$ added. (c) H-stripping voltammograms used to measure the ECSA of Pt catalyst. (d) Summary of calculated ECSA for catalysts.

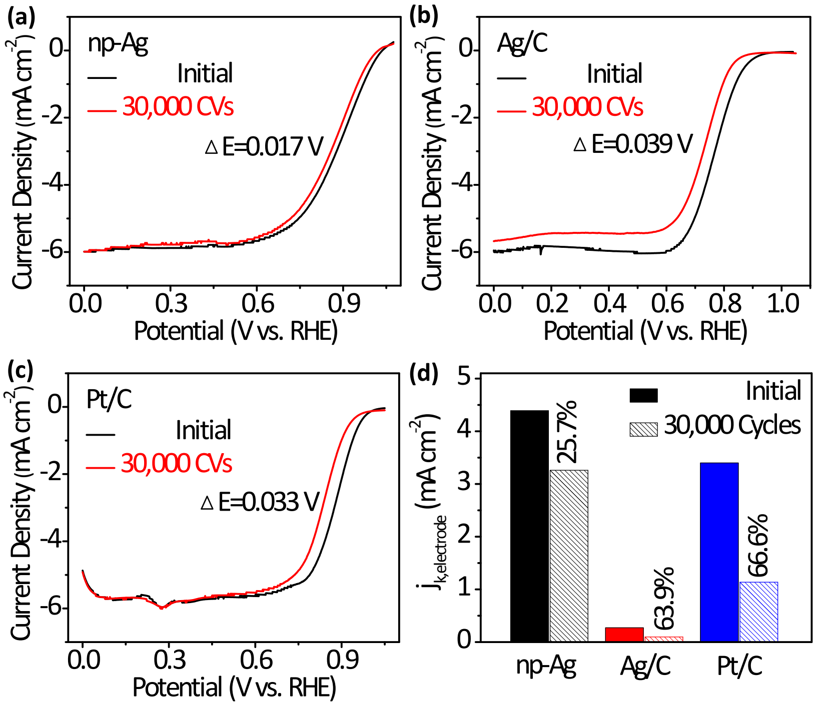

Figure S8. (a), (b), (c) Long-term degradation of ORR polarization curves with cycling for np-Ag, Ag/C and Pt/C, respectively. (d) Comparison of kinetic current density (j_k) of catalysts before and after the stability tests (@0.9V).

Table S1. Comparison of the ORR electrocatalytic activity of np-Ag to the recent reported pure Ag catalysts in alkaline media (0.1M KOH or NaOH).

Catalyst	Mass Activity (mA $mg^{-1}{}_{Ag}$)	Specific Activity (mA $cm^{-2}{}_{Ag}$)	Reference
NP Ag	2.0		*Fuel Cells* **2010**, *10*, 575.
np-Ag	-	0.024	*Adv. Funct. Mater.* **2015**, *5*, 1500149.
AgNW 25nm	6.2	0.085	*ChemSusChem* **2012**, *5*, 1619
AgNP 2.4nm	5.3	0.016	
Ag/C	0.425	0.0045	This work
np-Ag	6.90	0.068	This work

References

1 Ilhan, S.; Kahruman, C.; Yusufoglu, I. *J. Anal. Appl. Pyrolysis* **2007**, *78*, 363.

2 (a) Zhou, R.; Qiao, S. Z. *Chem. Mater.* **2014**, *26*, 5868. (b) Guo, J.; Hsu, A.; Chu, D.; Chen, R. *J. Phys. Chem. C* **2010**, *114*, 4324.

3 Zhou, Y.; Lu, Q.; Zhuang, Z.; Hutchings, G. S.; Kattel, S.; Yan. Y.; Chen, J. G.; Xiao. J. Q.; Jiao, F. *Adver. Energy Mater* **2015**, *5*, 1500149.

4 (a) Jeon, I.-Y.; Zhang, S.; Zhang, L.; Choi, H.-J.; Seo, J.-M.; Xia, Z.; Dai, L.; Baek, J.-B. *Adv. Mater.* **2013**, *25*, 6138. (b) Su, C.-Y.; Liu, B.-H.; Chi, Y.-M.; Kei, C.-C.; Wang, K.-W.; Perng, T.-P. *J. Mater. Chem. A* **2015**, *3*, 18983.

5 (a) Song, Y.-F.; Tsunashima, R. *Chem. Soc. Rev.* **2012**, *41*, 7384. (b) Douvas, A. M.; Makarona, E.; Glezos, N.; Argitis, P.; Mielczarski, J. A.; Mielczaeski, E. *ACS NANO* **2008**, *2*, 733. (c) Ju, F.; VanderVelde, D.; Nikolla, E. *ACS. Catal.* **2014**, *4*, 1358. (d) Han, Q.; He, C.; Zhao, M.; Qi, B.; Niu, J.; Duan, C. *J. Am. Chem. Soc.* **2013**, *135*, 10186.

6 (a) Kim, Y.; Shanmugam, S. *ACS Appl. Mater. Interfaces* **2013**, *5*, 12197. (b) Yang, M.; Choi, B. G.; Jung, S. C.; Han, Y.-K.; Huh, Y. S.; Lee, S. B. *Adv. Funct. Mater.* **2014**, *24*, 7301.